Mesoscale Surface Pressure and Temperature Features Associated with Bow Echoes

REBECCA D. ADAMS-SELIN AND RICHARD H. JOHNSON

Department of Atmospheric Science, Colorado State University, Fort Collins, Colorado

(Manuscript received 1 December 2008, in final form 26 June 2009)

ABSTRACT

This study examines observed mesoscale surface pressure, temperature, and wind features of bow echoes. Bow-echo events in the area of the Oklahoma Mesonet are selected for study to take advantage of high-resolution surface data. Thirty-six cases are identified using 2-km-resolution radar reflectivity data over a 4-yr period (2002–05); their surface features are interrogated using the mesonet data. Distinct surface features usually associated with squall lines, the mesohigh and cold pool, are found to also accompany bow echoes. A common surface pattern preceding bowing is identified. Prior to new bowing development, the mesohigh surges ahead of the convective line while the cold pool remains centered behind it. Surface winds shift to a ground-relative outflow pattern upon arrival of the mesohigh surge. Approximately 30 min later, a new bowing segment forms with its apex slightly to the left (with respect to the direction of system motion) of the mesohigh surge. The cold pool follows the convective line as it bows. This process is termed the ''pressure surge–new bowing'' cycle, and a conceptual model is presented. In one representative case, the surface signature of a gravity wave, identified through spatial and temporal filtering, is tracked. It is presumed to be generated by deep heating within the convective line. The wave moved at nearly 35 m s^{-1} and has heretofore been undetected in mesoanalysis studies. Two other distinct features, a sharp pressure rise and temperature drop, were also observed at all mesonet stations affected by the system. Possible explanations for these features in terms of a gravity current, gravity wave, or atmospheric bore are explored.

1. Introduction

The type of severe storm labeled as a ''bow echo'' has been recognized as a source of severe winds and strong downbursts since 1978, when T. T. Fujita first assigned the name to a class of small-scale, curved or quasi-linear convective systems. The bow echo's association with large swaths of damaging severe winds has been well documented from Fujita's original work (Fujita 1978) to the present (Johns and Hirt 1987; Houze et al. 1989; Przybylinski 1995; Evans and Doswell 2001; Klimowski et al. 2003; Wakimoto et al. 2006a,b). Severe, straight-line convective winds are potentially as hazardous as tornadoes to both life and property and often occur over a larger area (Johns and Hirt 1987; Przybylinski 1995). The most severe winds associated with bow echoes have been connected with low-level meso-gamma-scale vortices located within the bow itself (Weisman and Trapp 2003; Trapp and Weisman 2003; Wakimoto et al. 2006a,b). Severe winds can still occur along the entire bow-shaped convective line—in particular, at its apex—in addition to within the mesovortices (Trapp and Weisman 2003).

The theory of Rotunno et al. (1988) for structure and evolution of mesoscale convective systems (MCSs), as adapted to bow echoes by Weisman (1992, 1993), suggests that the lifetime and strength of a bow-echo system depend on the relative balance among vorticities generated by the horizontal buoyancy gradient at the front and back edges of the cold pool, the low-level environmental shear, and the rear inflow jet. The rear inflow jet initially develops in response to a midlevel mesolow just behind the convective updraft; the mesolow is generated by a vertical gradient in diabatic heating (i.e., latent heating in a mesoscale updraft overlying an evaporatively cooled downdraft; Smull and Houze 1987; Lafore and Moncrieff 1989). Over time, the jet expands rearward (Klimowski 1994) because of the horizontal buoyancy gradients associated with the back edge of the cold pool at the rear of the system (Weisman 1992, 1993). Increased rear inflow leads to an increase in evaporative cooling; the system's propagation speed surges in response. In

Corresponding author address: Rebecca D. Adams-Selin, HQ Air Force Weather Agency 2 WXG/WEA, 101 Nelson Dr., Offutt AFB, NE 68113.
E-mail: rebecca.selin.ctr@offutt.af.mil

DOI: 10.1175/2009MWR2892.1

Report Documentation Page

Form Approved
OMB No. 0704-0188

1. REPORT DATE	2. REPORT TYPE	3. DATES COVERED
26 JUN 2009		**00-00-2009 to 00-00-2009**

4. TITLE AND SUBTITLE	5a. CONTRACT NUMBER
Mesoscale Surface Pressure and Temperature Features Associated with Bow Echoes	5b. GRANT NUMBER
	5c. PROGRAM ELEMENT NUMBER
6. AUTHOR(S)	5d. PROJECT NUMBER
	5e. TASK NUMBER
	5f. WORK UNIT NUMBER
7. PERFORMING ORGANIZATION NAME(S) AND ADDRESS(ES) **Air Force Weather Agency,2WXG/WEA,101 Nelson Dr,Offutt AFB,NE,68113**	8. PERFORMING ORGANIZATION REPORT NUMBER
9. SPONSORING/MONITORING AGENCY NAME(S) AND ADDRESS(ES)	10. SPONSOR/MONITOR'S ACRONYM(S)
	11. SPONSOR/MONITOR'S REPORT NUMBER(S)

12. DISTRIBUTION/AVAILABILITY STATEMENT
Approved for public release; distribution unlimited

13. SUPPLEMENTARY NOTES

14. ABSTRACT
see report

15. SUBJECT TERMS

16. SECURITY CLASSIFICATION OF:			17. LIMITATION OF ABSTRACT	18. NUMBER OF PAGES	19a. NAME OF RESPONSIBLE PERSON
a. REPORT **unclassified**	b. ABSTRACT **unclassified**	c. THIS PAGE **unclassified**	**Same as Report (SAR)**	**17**	

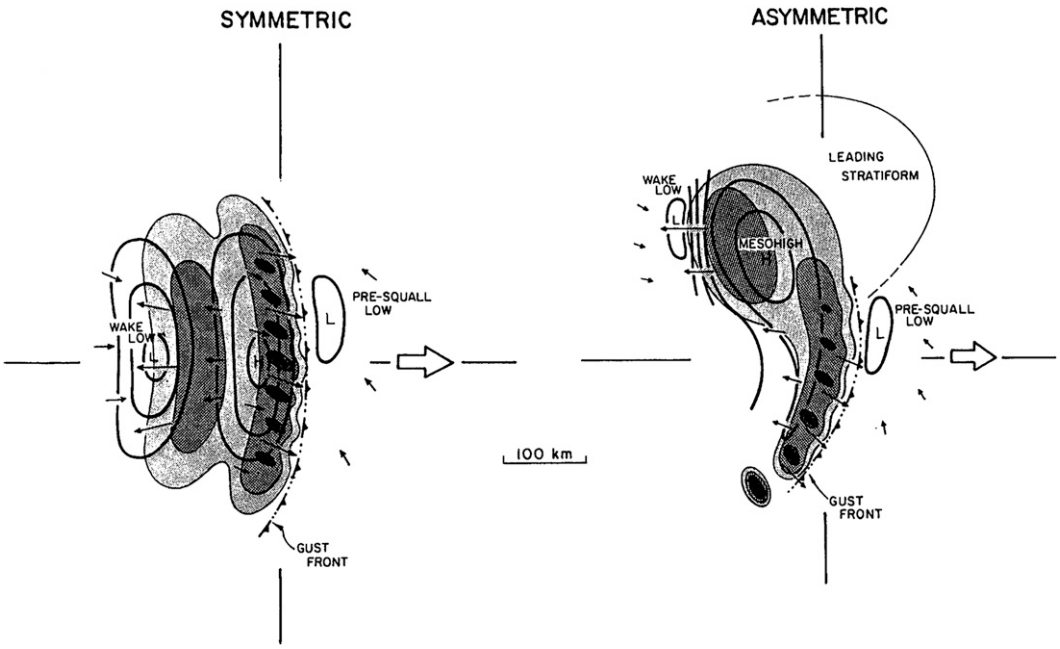

FIG. 1. Surface pressure features of a large squall-line MCS as it evolves from symmetric to asymmetric form (as in Houze et al. 1990). Large arrows show storm motion; small arrows indicate system-relative winds. The shading corresponds to increasing levels of radar reflectivity, with the heaviest being in the convective line. Figure is taken from Loehrer and Johnson (1995).

the Weisman studies, it is argued that portions of the cold pool occasionally become strong enough that their generated vorticity temporarily overwhelms the low-level shear vorticity. This lets the rear inflow jet descend to the surface, allowing for both a surge in surface winds as well as additional increase in propagation speed. The factors result in a convective line bowing out over time.

However, very little work has focused on the surface features, such as pressure and temperature anomalies, associated with bow echoes. This is primarily due to the lack of sufficiently dense observational datasets. The arrangement of these anomalies associated with larger squall-line MCSs is highly recognizable (Fig. 1). A surface mesohigh, primarily hydrostatically induced by evaporation and sublimation, is located beneath the strongest downdraft within the system, just behind the convective line (Fujita 1955; Wakimoto 1982; Johnson and Hamilton 1988). The cold pool is typically collocated with this feature. The surface wake low is positioned at the back edge of the stratiform precipitation region and is generated by subsidence aloft in the descending rear inflow jet (Johnson and Hamilton 1988; Stumpf et al. 1991). The warmer subsiding air is only occasionally able to penetrate through the cold, stable, postconvection boundary layer to the surface, producing phenomena termed ''heat bursts'' (Johnson 1983). A presquall mesolow is found in advance of the convective line, induced by upper-level subsidence (Hoxit et al. 1976; Johnson and Hamilton 1988). Over time, the stratiform precipitation region, along with the mesohigh and the cold pool, shifts to the left of the direction of system motion, as in ''asymmetric'' in Fig. 1 (Houze et al. 1990; Skamarock et al. 1994; Loehrer and Johnson 1995; Hilgendorf and Johnson 1998); although occasionally leading or parallel regions of stratiform precipitation, mesohigh, and cold pool are also seen (Parker and Johnson 2000). The extent of application of these patterns to bow echoes is currently unknown.

Recent simulations have suggested that these squall-line airflow and surface pressure patterns, particularly the mesohigh and presquall mesolow, can be at least partially attributed to gravity current and gravity wave dynamics produced by temperature perturbations within the convective line and stratiform precipitation region (Charba 1974; Schmidt and Cotton 1990; Nicholls et al. 1991; Pandya and Durran 1996; Haertel and Johnson 2000; Haertel et al. 2001; Fovell 2002). According to Nicholls et al. (1991), Haertel et al. (2001), and Fovell (2002), multiple gravity waves and currents are often generated by a single squall-line MCS. The initial profile of deep heating throughout the troposphere associated with a convective line generates a fast-moving, deep gravity wave, indicated at the surface by a region of low pressure spreading quickly away from the system

(Nicholls et al. 1991; Fovell 2002). The low-level cooling associated with both a mature convective line and a stratiform region (Gallus and Johnson 1991) produces a slow-moving gravity wave that often travels at a speed similar to that of the MCS (Haertel and Johnson 2000). Both of these gravity waves do result in some net displacement of air surrounding the system; this displacement can make the surrounding environment more favorable for new convection (Mapes 1993).

The low-level cooling also yields a cold pool that spreads along the ground as a gravity current (Charba 1974). Depending on the stability of the low-level atmosphere in advance of the squall line, the gravity current may make a transition to a bore or gravity wave with appropriate increase in speed (Parker 2008). After such a transition, the average observed difference in potential temperature between the cold pool and the environment would be expected to be smaller at the surface than aloft. This was observed in a Bow Echo and Mesoscale Convective Vortex Experiment (BAMEX) observational study of all types of MCSs, bow echo and squall line, by Bryan et al. (2005). Further BAMEX observations have produced differing results regarding the effects of surface stable layers. Jorgensen et al. (2004) attributed the lack of strong surface winds in the bow echo observed during BAMEX intensive observing period 7 to a strong stable layer in advance of the system. However, Bryan and Weisman (2006) noted that severe surface winds, and a strong surface-based cold pool, can occur with an elevated MCS if the air is cooled enough to allow it to descend to the surface.

It is still uncertain how fully both these squall-line surface patterns, and gravity current and gravity wave dynamics, can be applied to bow echoes. The goals of this study are to examine the similarity of these features to those associated with larger squall-line MCSs, to determine whether systematic behavior in these fields exists, and to decide if that behavior sheds light on bow-echo dynamics and predictability. Until recently, surface observing networks have not been dense enough to capture patterns associated with such small-scale features. However, the Oklahoma Mesonet, established in 1994, now provides observations on detailed spatial (40–50 km) and temporal (5 min) scales (Brock et al. 1995). This study utilizes the mesonet, in combination with the Weather Services International, Inc., (WSI) National Weather Service radar data (NOWrad), in an attempt to find a common pattern that precedes development of a new bow and its typically attendant severe winds. Such a pattern would be useful for both operational and research-oriented meteorology.

The data and analysis methods used, as well as the criteria determined to be necessary for a bow echo, are detailed in section 2. Two bow-echo case studies are examined in detail in section 3. The surface temperature, pressure, and wind patterns evident in these cases were representative of a large majority of cases, and a conceptual model of these patterns is shown in section 4. In section 5, one of the case studies is examined in detail for possible evidence of gravity waves and gravity currents.

2. Data and analysis procedures

a. Oklahoma Mesonet

To resolve surface features on the scale of bow echoes, an observing network of higher spatial and temporal resolution than the current aviation routine weather report (METAR) network is required. The Oklahoma Mesonet provides environmental observations every 5 min from over 110 stations across Oklahoma (Fig. 2). Observed variables utilized in this study include 1.5-m air temperature, 1.5-m relative humidity, station pressure, and average 5-min, 10-m wind speed and direction.

The effect of station elevation was removed from the pressure dataset using the method of Loehrer and Johnson (1995). The station pressure was adjusted to 356.5 m, the mean height of the mesonet stations. Diurnal and semidiurnal tidal oscillations were removed from the station pressure data using the procedure described in Johnson and Hamilton (1988). Because the focus of this study is on mesoscale features, synoptic-scale effects were removed by applying a Lanczos high-pass Fourier filter (Duchon 1979) to the data. Its response function is shown in Fig. 3. Low-frequency oscillations with periods of greater than 82.4 h, or 2 times the length of a pendulum day for the average latitude in Oklahoma, were considered to be synoptic-scale phenomena and irrelevant for this study and thus were removed by this filter.

To further enhance the mesoanalyses, a time-to-space transformation (Fujita 1955) was performed on the data during the periods that bow echoes were within the state. For the purpose of this analysis, meteorological fields associated with the bow echoes were assumed to be approximately steady state for 15-min periods (to coincide with the 15-min WSI NOWrad radar data). After determining the system's speed and direction of motion, 5-min observations from stations in proximity to the bow echoes were translated into a line at each station using the procedure of Knievel and Johnson (1998). Each system's velocity was found by examining the Weather Surveillance Radar-1988 Doppler (WSR-88D) Next Generation Weather Radar (NEXRAD) radar data, downloaded from the National Climatic Data Center Hierarchical Data Storage System (NCDC HDSS,

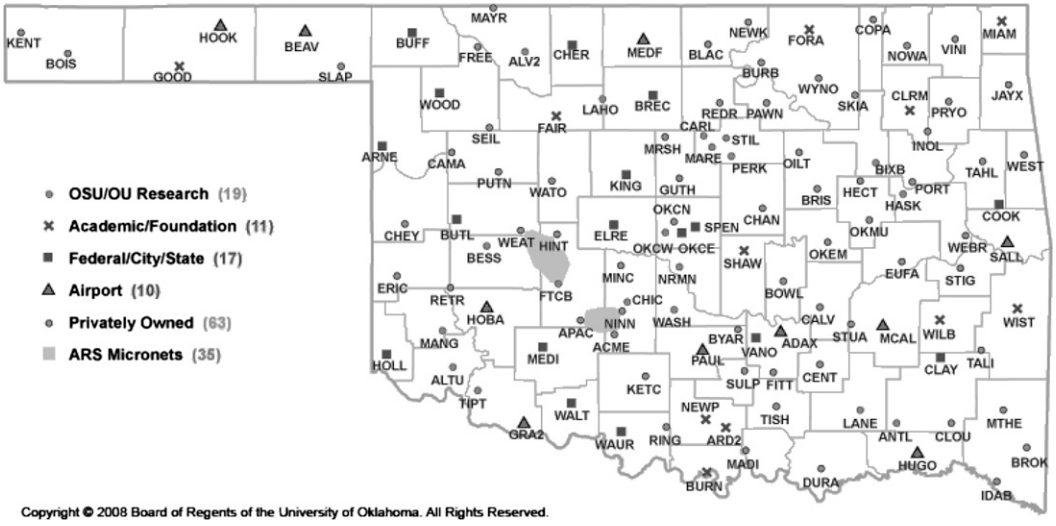

FIG. 2. Oklahoma Mesonet stations as of 2006 (found online at www.mesonet.org/images/siteIDs.gif).

accessed online at http://has.ncdc.noaa.gov), and using the heading-speed tool in the Advanced Weather Interactive Processing System. The time-to-space transformation was only applied over a movable, latitude- and longitude-defined rectangle, redefined every 15 min, which followed the bow echo.

After the data field was enhanced by this procedure, the observations were then objectively analyzed using the multiquadric interpolation scheme. Nuss and Titley (1994) found that this scheme performed better than the more commonly used Barnes (1973) or Cressman (1959) schemes, in particular for small-scale features.[1] The smoothing and multiquadric parameters were set to 0.000 005 and 1.5, respectively. These values were found through repeated experimentation to best retain the tight gradients associated with convection. Because this scheme does not perform well in regions with sparse observations, results in the Oklahoma Panhandle, where only six mesonet stations are located, were excluded from the analysis. The newly gridded data were then read into the General Meteorological Package (GEMPAK) to produce contoured fields.

b. National mosaic radar reflectivity data

WSI NOWrad mosaic composite reflectivity data at 15-min resolution, from the National Center for Atmospheric Research Mesoscale and Microscale Meteorology Division (MMM) archive (available online at http://www.mmm.ucar.edu/imagearchive/WSI), were added to the GEMPAK analysis. [For a description of WSI NOWrad data, see http://www.mmm.ucar.edu/imagearchive/WSI/docs/NOWradDescriptionWSICorp.txt; Parker and Knievel (2005) contains a discussion of its strengths and weaknesses.] When this study began, data in native WSI NOWrad format (easily visualized using GEMPAK) were only available for the full years 2002–05. To remain consistent throughout the study, the analysis was limited to those years. Plots of high-pass-filtered potential temperature, surface winds, and adjusted surface pressure, overlaid on radar data, were produced at 15-min intervals for all bow-echo cases found over this 4-yr period.

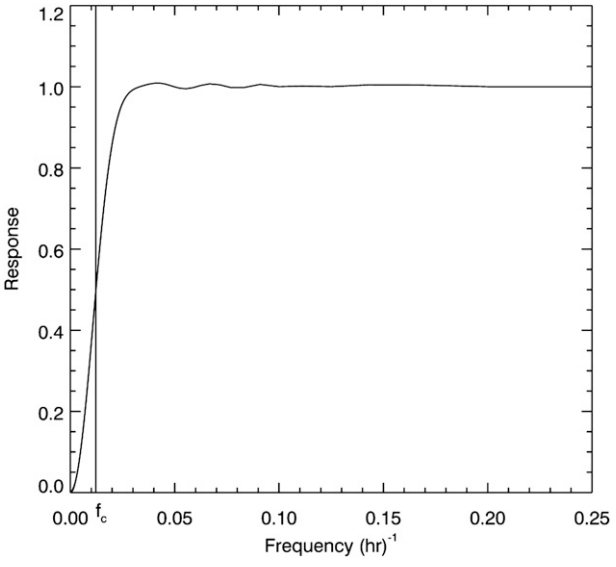

FIG. 3. Response function for the 81-point width high-pass Lanczos filter. The cutoff frequency f_c is one full wave (one synoptic high–low pressure couplet) per 82.4 h, or 0.0121 h^{-1}.

[1] For robustness, data fields were also objectively analyzed using the Barnes method, with a number of different critical radii. Results very similar to those found using the multiquadric method were achieved.

c. Bow-echo criteria

The MMM online animated image archive (http://www.mmm.ucar.edu/imagearchive) was utilized to narrow the 4 yr of data to possible bow-echo events. These events were then examined in more detail using animations of the WSI NOWrad mosaic radar data. If a radar feature met the necessary criteria (discussed below) it was included as one of the cases. Tracking of the feature began when either convection started or when the bow apex entered the state. Tracking of the feature ended with the exit of the stratiform precipitation region to another state, the conversion or merging of the bow echo into a larger system, or the dissipation of the convection. Here, start (dissipation) of convection was established by the appearance (dissipation) of 50-dBZ echoes. Fourteen days of radar data were missing from this archive, during the period 9–22 June 2002.

The definition for a bow echo used in this study is largely based on the work of Klimowski et al. (2000). To be designated as a bow echo, a feature must appear ''bow or crescent-shaped'' on the radar return and display a strong gradient in reflectivity at the leading edge of the bow. As in both Fujita (1955) and Klimowski et al. (2000), bow echoes must display characteristics of being ''outflow dominated'' with the radius of curvature of the bow as viewed by radar decreasing with time. The American Meteorological Society *Glossary of Meteorology's* definition of a bow echo sets an upper size threshold at 200 km (Glickman 2000). None of the bowing segments examined in this study were larger.

Additional restrictions to this definition were necessary as a result of the 15-min temporal resolution of the WSI NOWrad data. The system also must be large enough to ensure that the mesonet could adequately sample any surface pattern associated with the bow. Thus, the following four constraints served as bow-echo selection criteria for this study:

1) a strong reflectivity gradient at the leading edge of the bow must be present,
2) the bow or crescent shape of the radar echo must endure for at least 1 h,
3) new bowing development, the period during which the radius of curvature of the echo decreases with time, must persist for at least 30 min during this same period, and
4) during these time periods, the system must be large enough to cover the average distance between two mesonet stations, approximately 50 km, and the apex of the bow must be within Oklahoma (excluding the panhandle).

TABLE 1. Relationship between pressure surge and new bowing as represented by the number of bowing episodes that were preceded by (before), simultaneous to (simul), followed by (after), and not associated with (none) surges of the surface mesohigh. Surges not followed by new bowing (Surge/no bow) are also indicated. Only new bowing that, at its start, was both larger than 50 km and inside the state (a ''bowing episode'') was included.

Before	Simul	After	None	Tot	Surge/no bow
24	8	3	4	39	8
61.5%	20.5%	7.7%	10.3%	100.0%	

Thirty-six total bow-echo cases were identified during the 2002–05 period using these criteria. It is possible, however, for one bow-echo case to contain several bowing segments. These multiple segments could occur at the same time and be located within the same bow, such as the serial derecho described by Johns and Hirt (1987), or could appear sequentially in time. Each instance of new bowing development within one bow-echo case was referred to as a ''bowing episode.'' A total of 39 bowing episodes were confirmed within the time period of this study (Table 1).

3. Case studies

A total of 36 cases involving 39 bowing episodes were studied by animating the radar reflectivity, pressure, and temperature fields and examining their interrelationships. In this section, two representative cases are presented. Figures 4 and 6 display composite radar images of these two cases, overlaid with high-pass-filtered surface sustained winds, potential temperature, and adjusted pressure. The WSR-88D radial velocity data (converted to a storm-relative framework) from stations KTLX (Norman, Oklahoma) and KVNX (Enid, Oklahoma) were also examined. Because the data were obtained from the NCDC HDSS archive, only the lowest four elevation angles (0.50°, 1.50°, 2.40°, and 3.40°) were available.

a. 13 March 2003 bow echo

Convection first initiated at 0215 UTC in north-central Oklahoma, and a convective line approximately 125 km in length was in place by 0230 UTC (Fig. 4a), with continued development evident at 0345 UTC (Fig. 4b). Winds ahead of the storm system were generally from the south by 0345 UTC, providing inflow; wind observations from within the convective line were from the north-northwest. Figure 4c, at 0515 UTC, displays the arrangement of the mesohigh and cold pool in relation to the convective line prior to the start of new bowing. The mesohigh was centered just behind this

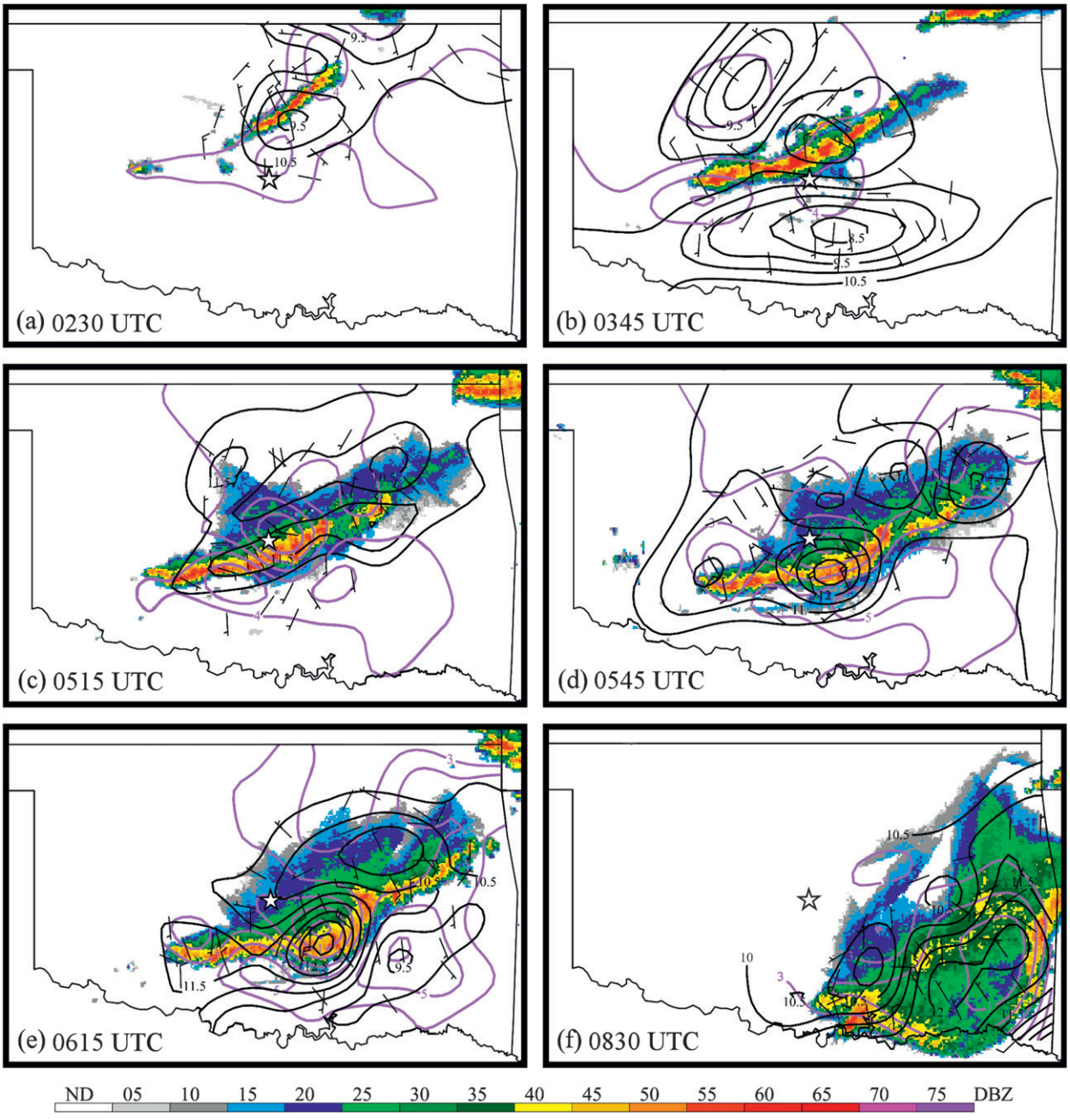

FIG. 4. High-pass-filtered potential temperature (purple contours; 1°C), surface wind (black barbs), and adjusted pressure (black contours; 0.5 hPa) from (a) 0230, (b) 0345, (c) 0515, (d) 0545, (e) 0615, and (f) 0830 UTC 13 Mar 2003. The WSI NOWrad base reflectivity scale is given at the bottom of the figure. The pressure surge and new bowing development are displayed in (d) and (e), respectively. The position of KTLX is marked by a star.

convective line, with a cold pool approximately collocated with the mesohigh. Surface winds ahead of the convective line were still predominately southerly. Winds within the convective line were more variable but were generally northerly.

By 0530 UTC (not shown), the mesohigh shifted farther toward the southern end of the convective line. Examination of the KTLX WSR-88D storm-relative radial velocity data (not shown) revealed the existence of a rear inflow jet, located in the southern third of the convective line and approximately in the center of the mesohigh. The jet was approximately 50 km in width and only extended rearward to the trailing edge of the convective line. There was a small area of winds exceeding

20 m s^{-1} at 1.5 km. This feature first appeared at 0516 UTC. It is uncertain if that was when the inflow first developed, or when the system moved far enough away from the KTLX radar for the highest available elevation angle to be able to sample this feature.

Figure 4d shows the noticeable mesohigh surge partially ahead of the convective line at 0545 UTC, with slight bowing of the convective line. The cold pool remained centered behind the convective line with isotherms parallel to it. A 20 m s^{-1} rear inflow jet maximum was still located at approximately 1.5 km (not shown). It was also collocated with the center of the surging mesohigh. Stations located in advance of the convective line but within the mesohigh surge switched from southerly inflow to northerly flow. Later evaluation (see section 5b) of data time series showed that the surface winds shifted with the mesohigh surge.

By 0600 UTC, 20 m s^{-1} winds were also observed at 1 km (not shown), appearing to indicate a descending rear inflow jet. Thirty minutes later (0615 UTC, Fig. 4e), an area of new bowing developed just to the northeast of the axis of the mesohigh surge. The cold pool expanded outward with the new bow but remained centered behind the convective line. Its minimum potential temperature decreased by approximately 1°C since the mesohigh surge. Surface winds located within the pressure gradient at the leading edge of the mesohigh shifted direction to north-northwest. At this point the leading edge of the mesohigh pressure gradient was still ahead of the convective line. There was still a small region of 20 m s^{-1} storm-relative radial winds visible in the KTLX WSR-88D data at approximately 1 km above the ground (not shown), but it was likely that the strongest winds had descended to the surface. A 17 m s^{-1} wind gust was reported at station ADAX (see Fig. 2 for station location) at 0600 UTC. Stratiform precipitation increased considerably at this time. The rear inflow jet expanded rearward as the stratiform region increased in size (not shown).

About 2 h after the new bowing episode developed, the convective line began to dissipate as the bow expanded (0830 UTC, Fig. 4f). An enhanced secondary band of stratiform precipitation had developed by this time, which along with the cold pool was centered in the northern half of the bowed portion of the convective line. The one remaining station in the prestorm region reported winds shifting clockwise from south to northwest as the system approached, with other nearby stations all reporting northwest flow. The cold-pool isotherms had remained parallel to the convective line over the past 2 h (not shown). The mesohigh was centered behind the convective line close to the cold pool, although it was elongated partially southwestward. Both features would remain centered behind the convective line as the system dissipated.

Possible mechanisms for the mesohigh surge associated with the 13 March bow echo are explored in section 5 by referring to a time series of the surface observations (Fig. 5) from station VANO in south-central Oklahoma on 13 March 2003 (see Fig. 2 for station location). However, here we refer to this time series to point out limitations of the objective analysis in representing the sharp mesoscale pressure gradients associated with the storm. Based on an average system speed of 17.3 m s^{-1}, calculated using the time of arrival of precipitation at stations CHAN and CALV (see Fig. 2 for station location), a time–space transformation of the interval between the initial pressure rise (0535 UTC; ''b'' in Fig. 5) and the pressure peak (0555 UTC; ''d'' in Fig. 5) yields 20.8 km. The width of the same pressure gradient in Fig. 4d, however, is approximately 60 km. It is clear that the multiquadric interpolation does not fully capture the true sharp pressure gradient. Further adjustment of the smoothing and multiquadric parameters did not improve this disparity. Thus, although the principal results of this study are not compromised by this deficiency, details of the surface analyses—namely, sharp gradients—are not fully resolved by the objective analysis scheme.

b. 24 May 2003 bow echo

At 1200 UTC (not shown), an already-developed convective line, oriented southwest–northeast, entered the northwest portion of Oklahoma. By 1245 UTC, more than half of the length of the convective line was within the mesonet, and a mesohigh and cold pool were both evident (Fig. 6a). In this case, it appears as though these features were located just behind the southwestern end of the convective line, although given the proximity of the storm to the boundary of the mesonet, the exact locations are uncertain. The pressure gradient at the leading edge of the mesohigh was slightly ahead of the convective line, and winds at stations within that gradient were indicating northwest flow. Other stations ahead of the system reported generally south or southwest winds flowing into the system. KVNX WSR-88D data (not shown) showed a well-developed rear inflow jet of greater than 20 m s^{-1} stretching vertically from 1.5 to 5.0 km. It was located in the southern third of the convective line, just to the northeast of the mesohigh, and extended approximately 100 km behind the trailing edge of the convective line.

The mesohigh surged partially ahead of the convective line at 1300 UTC (Fig. 6b). The cold pool remained behind the convective line with its isotherms parallel to it. It did not strengthen at this time but appeared to be more centered behind the convective line than earlier.

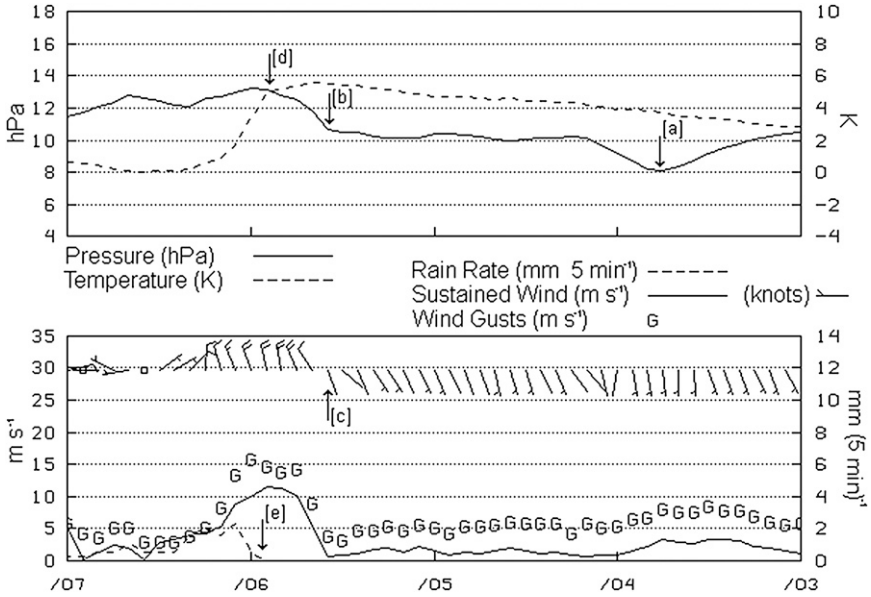

FIG. 5. Time series display of high-pass-filtered data for station VANO, which experienced both the pressure surge and the newly bowed segment of the bow echo. Time increases to the left, from 0300 to 0700 UTC 13 Mar 2003. (top) Potential temperature (K; dashed line; right scale) and adjusted pressure (hPa; solid line; left scale). (bottom) Sustained winds (1 kt $\approx$ 0.5 m s^{-1}; barbs), sustained wind speed (m s^{-1}; solid line; left scale), unfiltered wind gusts (m s^{-1}; "G" labels, left scale), and unfiltered precipitation rate [mm (5 min)$^{-1}$; dashed line; right scale]. Arrow a is the dip in pressure signifying the passage of the fast-moving wavelike feature (0345 UTC). Arrows b and c are the start of the sharp pressure rise and the wind shift (0535 UTC). Arrow d is the sharp potential temperature drop (0555 UTC) and arrival of the cold pool. Arrow e is the start of precipitation, at the same time.

At this time, 20 m s^{-1} rear inflow jet winds have descended to 1.2 km, approximately collocated with the mesohigh. The rearward extent of the jet cannot be seen because a large portion of it is perpendicular to the radar velocity radial. Surface winds at the very leading edge of the mesohigh pressure gradient—over 50 km in advance of the convective system—have shifted to the northwest. Review of data time series at nearby station BREC (not shown; see Fig. 2 for station location) showed that the wind shift occurred simultaneously with the arrival of the mesohigh surge.

Within 15 min (1315 UTC; Fig. 6c), new bowing developed to the northeast of the mesohigh surge. The cold pool remained centered behind the system and at the same strength, although it did surge forward with the line as it bowed. At this time, there were no mesonet stations within the pressure gradient on the leading edge of the mesohigh ahead of the system; two stations just in advance of the gradient reported southerly or southwesterly inflow. Doppler radar data revealed the 20 m s^{-1} winds in the rear inflow did not descend to the surface (not shown).

By 1500 UTC (Fig. 6d), the radius of curvature of the convective line had increased. The mesohigh was located behind the convective line toward its southwest end. The cold pool was still centered behind the convective line. Winds in the pressure gradient in advance of the system were generally from the north. Most of the winds were oriented perpendicular to the KTLX radar velocity radial, and therefore discussion of the WSR-88D data cannot be included with this bowing episode. At 1515 UTC, the mesohigh once again surged ahead of the convective line (Fig. 6e). The cold pool remained centered behind the convective line, although its leading gradient did strengthen slightly. The convective line bowed slightly at this time, although not to the full extent that it did later. The two stations (NINN and CALV; see Fig. 2 for station location) located in the pressure gradient at the leading edge of the mesohigh still reported southwesterly inflow, although they were at the very front of this gradient. The wind shifted at station NINN 5 min later and at station CALV 15 min later.

At 1545 UTC (Fig. 6f), the convective line fully bowed out, with the new apex to the northeast of the original mesohigh surge. The cold pool was centered behind this new bowing segment and cooled by 1°C since the mesohigh surge. The mesohigh was still located at the southern end of the convective line, but was eclipsed by the new bowing segment. Stations near the convective line

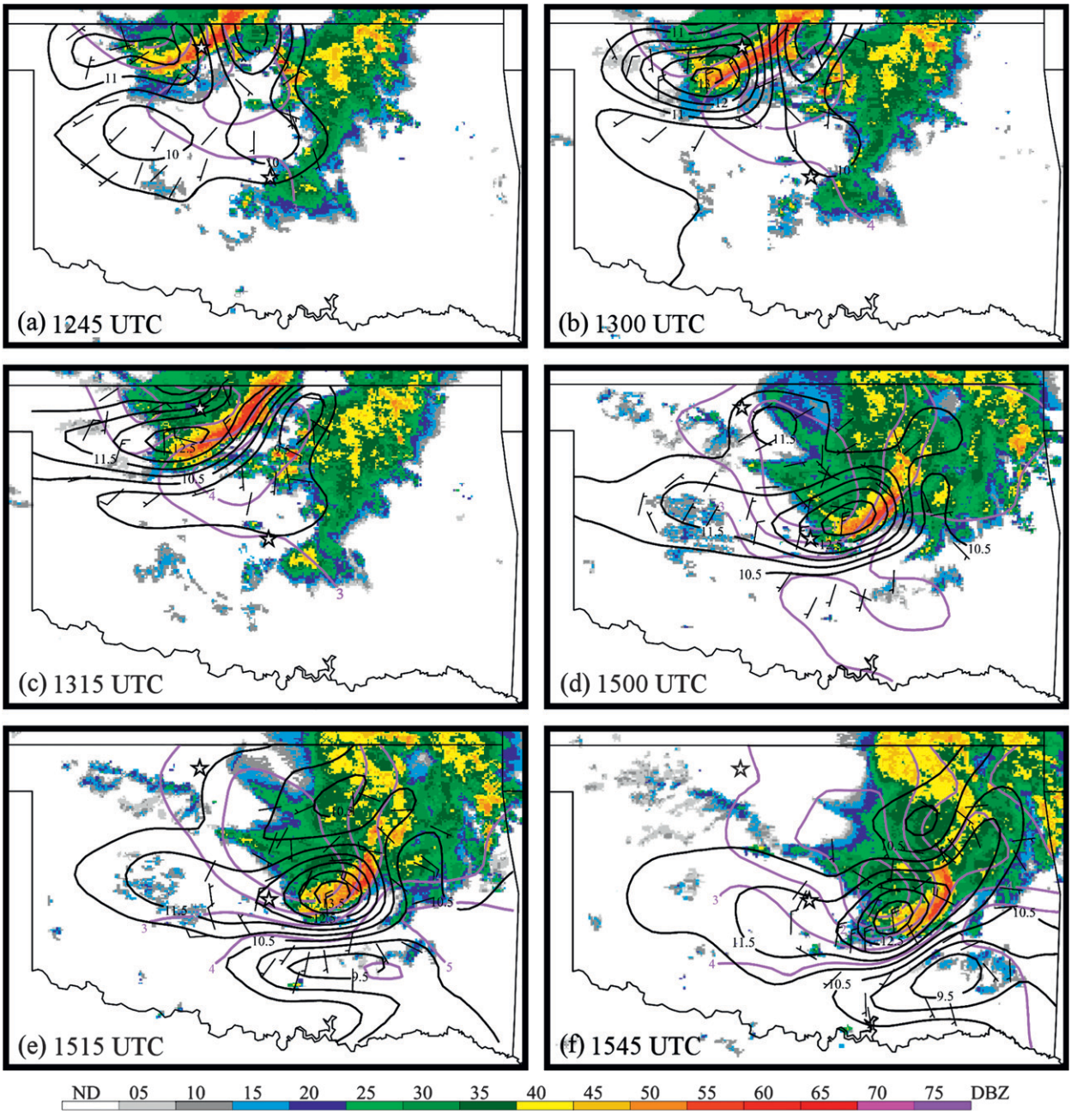

FIG. 6. As in Fig. 4, but at (a) 1245, (b) 1300, (c) 1315, (d) 1500, (e) 1515, and (f) 1545 UTC 24 May 2003. The pressure surges are in (b) and (e); the new bowing development is in (c) and (f). The star in northwest (central) Oklahoma is the KVNX (KTLX) radar.

and in the leading pressure gradient reported northwesterly flow. By 1715 UTC (not shown), the system exited the state while dissipating.

4. Surface pressure and temperature pattern synopsis

An examination of all bowing episodes was conducted to find recurring mesoscale surface pressure, temperature, or wind patterns. The existence of features often associated with linear MCSs, such as the postsystem wake low and warm region, presquall mesolow and warm region, and mesohigh and cold pool, were all observed. However, repeatable patterns of low pressure and warm temperature anomalies could not be established because the positioning and intensity of these features varied widely over the lifetime of each bow echo. A recurring pattern that could be identified was

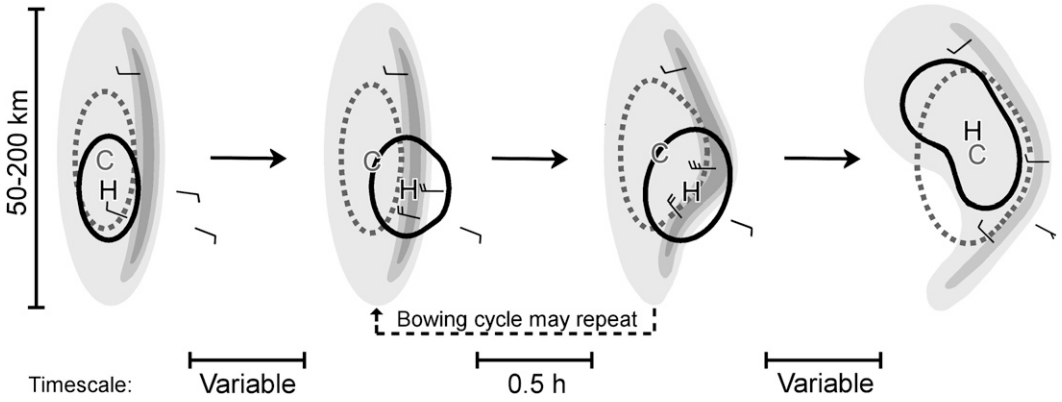

FIG. 7. Conceptual model for stages 1–4 of the relationship between pressure surge and new bowing. Shading roughly corresponds to radar reflectivity levels of 20, 40, and 50 dB*Z*. The dashed gray (solid black) contour surrounds the cold pool (mesohigh); C (H) is the point of lowest (highest) temperature (pressure) perturbation. Frequently observed surface winds and length and time scales are noted. Stages of development are the initial formation of convective line (stage 1), pressure surge ahead of convective line (stage 2), period of new bowing (stage 3), and dissipation (stage 4).

the surging of the mesohigh in advance of the convective line preceding bowing, which is depicted in the conceptual model shown in Fig. 7.

Stage 1 (Fig. 7) illustrates the arrangement of a bow-echo system following the formation of the full (>50 dB*Z*) convective line. The initiation of each convective line, mesohigh, and cold pool in this study varied widely. However, at some point after convective line formation but before new bowing development, the cold pool is typically centered behind the convective line with the mesohigh no more than 50 km to its south. Because every case studied had at least partially a north–south orientation, the terminology of north (south) will be used here to denote the left (right) ends of the line as viewed toward the direction of motion. In general, the mesoscale surface winds in advance of the system are from the east or southeast, providing inflow. Within the pressure gradient on the leading edge of the mesohigh, as well as near the convective line, the winds are generally dominated by flow in the direction of motion of the storm.

Stage 2 (Fig. 7) is characterized by a surge of the mesohigh wholly or partially ahead of the convective line, south of its center. The line might bow slightly at the same time, although bowing has not necessarily yet occurred. The cold pool, expanded slightly from the previous stage, remains centered behind the convective line. The transition of southeasterly flow to westerly flow occurs within the pressure gradient on the leading edge of the mesohigh as it moves ahead of the convective line during the surge. Winds within this gradient shift clockwise, becoming perpendicular to the convective line.

Stage 3 illustrates the development of new bowing, which expands the convective line to almost eclipse the mesohigh. The bow apex is north of the mesohigh surge, although the new bowing often includes the southern tip of the convective line. The cold pool remains centered behind the convective line and expands as it bows. Winds within the mesohigh pressure gradient are still oriented perpendicular to the convective line. The apex of the new bow is north of the mesohigh in every case examined that exhibited the surging behavior. Reasons for this displacement are yet unclear.

In 19 of the 24 bowing episodes with a mesohigh surge prior to new bowing development, the cold pool strengthened at some point during stages 2 or 3. The timing of this strengthening varies; it occurred with approximate equal frequency during the surge, during new bowing, and after new bowing development. In 5 of 24 episodes, the cold pool did not strengthen at all. It is possible that this lack of strengthening, at least at the surface, is due to a stabilizing low-level environment in advance of the system—in particular, at night. Observations above the surface would be necessary to examine the vertically integrated behavior of the cold pool, although further discussion of possible diurnal effects on the cases' cold pool strengths is in section 5b.

Stage 4 shows the dissipation of the convective line. In general, the mesohigh shifts behind the center of the bow apex into the stratiform precipitation region. In the context of the symmetric/asymmetric MCS patterns defined by Houze et al. (1990), if the stratiform region is situated symmetrically behind the rest of the convective line, the mesohigh will be as well. However, with an asymmetrically organized stratiform region the mesohigh typically moves northward to be collocated with the most intense stratiform rain. The cold pool remains

centered behind the convective line, although it shifts farther rearward into the stratiform region. Winds within the convective line and the pressure gradient in advance of the mesohigh are still westerly and perpendicular to the convective line.

The behavior described in stages 2 and 3 is termed the ''pressure surge–new bowing'' process. A majority of bowing episodes examined in this study, 61.5%, exhibited this behavior (Table 1). A number of cases even exhibited multiple cyles of pressure surge–new bowing before dissipating (indicated by the dashed line in Fig. 7), including the 24 May 2003 case described above. It is possible that the frequency of episodes appearing to exhibit simultaneous new bowing and pressure surge (20.5%, Table 1) could have been decreased had higher-temporal-resolution radar data been available. A full 89.7% of cases displayed some form of mesohigh surging, hinting that this plays an important role in the bowing process.

The time intervals between stages 1 and 2, as well as between 3 and 4, varied widely among the cases examined; on average, periods of 30–60 min for the first interval and 60–180 min for the third interval were observed. The interval between stages 2 and 3 was less variable, with a mean of 30 min among cases exhibiting the pressure surge–new bowing behavior, as shown in Fig. 8; the median was 15 min. The standard deviation was 21.2 min, with the maximum and minimum intervals being 90 and 15 min, respectively.

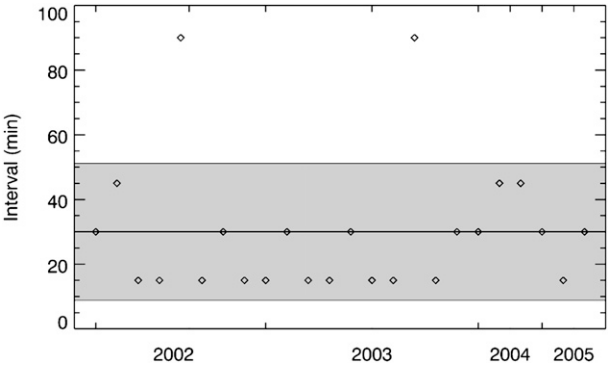

FIG. 8. Scatterplot of the interval between the pressure surge and new bowing development in bow echoes that exhibited the ''pressure surge–new bowing'' process. The thick horizontal line at 30.0 min is the mean; thin horizontal lines and the shaded area are the mean plus or minus one standard deviation (21.2 min).

5. Discussion of possible gravity waves associated with the 13 March 2003 bow echo and mesohigh surge

Surface pressure and temperature patterns typically associated with squall-line MCSs can be largely attributed to gravity current and wave dynamics connected with deep convective heating and evaporatively cooled downdraft outflows (Schmidt and Cotton 1990; Nicholls et al. 1991; Haertel and Johnson 2000; Haertel et al. 2001; Fovell 2002). Observations from the 13 March 2003 case were chosen to examine the role of gravity currents and waves in bow-echo evolution. This case was the only case with a convective line that fully initiated and at least partially dissipated within the mesonet while isolated from other convection. Station time series, and plots of surface pressure, are used to infer gravity current and gravity wave generation and subsequent propagation.

a. Fast-moving gravity wave generated by deep heating

In a theoretical study by Nicholls et al. (1991), a gravity wave induced by deep tropospheric heating throughout the troposphere generates a small low pressure region at the surface that spreads quickly (approximately 30–40 m s^{-1}) away from the heat source. The low pressure is produced by an outward-propagating band of subsidence warming associated with the first internal mode of heating (also see Mapes 1993; Fovell 2002). The surface manifestation of this mode has heretofore not been documented. However, the mesoscale filtering applied to the 13 March 2003 case has allowed this feature to be observed clearly for the first time.

Figures 4a and 4b display the initiation of the convective line on 13 March 2003 (0230 UTC; Fig. 4a), and the fully formed convective line prior to development of the trailing stratiform precipitation region (0345 UTC; Fig. 4b). At 0230 UTC there is a low pressure region coincident with the developing convective line. By 0345 UTC this low pressure has separated into two centers that have moved rapidly north and south of the source. The low pressure ahead of the convective line may in part be related to the presquall mesolow identified by Hoxit et al. (1976), a quasi-permanent feature they attribute to subsidence induced by deep convection in the convective line. However, it is clear that there is a rapidly propagating component to this feature. Estimates of the propagation speed will be presented later.

From examination of the time series at station VANO (Fig. 5), at approximately 0345 UTC (marked by ''a''), there is a temporary 2-hPa decrease in pressure, with very little accompanying wind or temperature signature. This appears to be the passage of an elevated, fast-moving, deep gravity wave. These dips in pressure, unattended by wind or temperature perturbations, were noted at almost all stations impacted by the bow echo (Fig. 9a). The isochrones in Fig. 9a display a rapidly propagating wavelike feature, moving in the direction

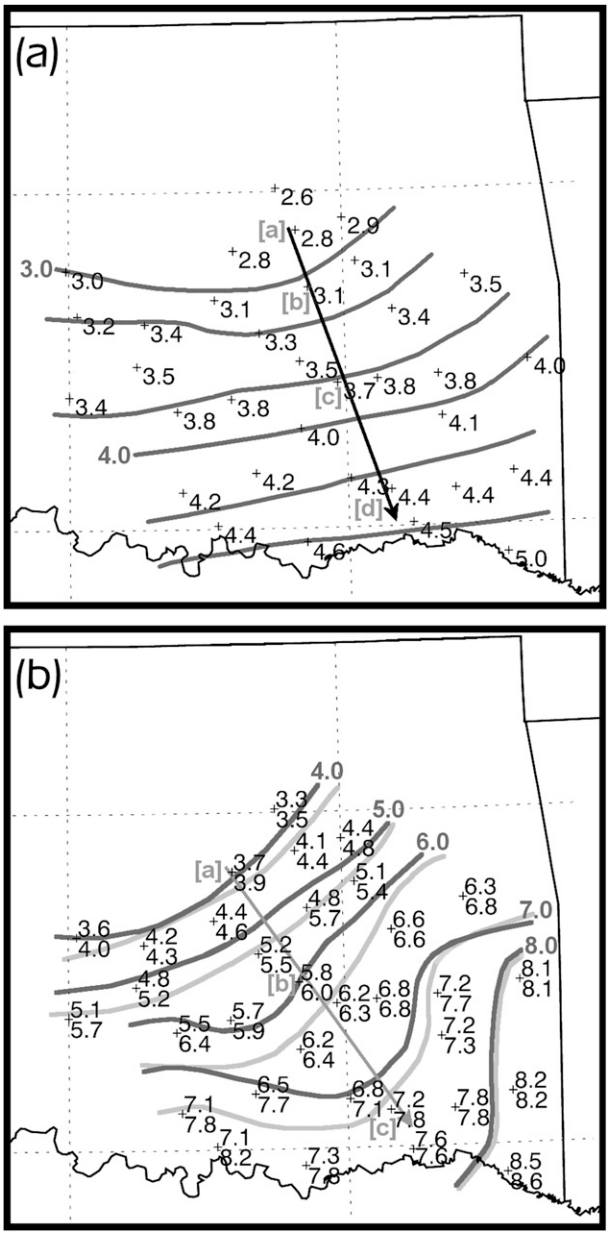

FIG. 9. (a) Isochrones (contoured every 20 min) of the pressure dip associated with the fast-moving wavelike feature, thought to be a gravity wave generated by deep heating in the 13 Mar 2003 bow-echo convective line in southeast Oklahoma. The time at which the feature reached each affected station is noted (some stations are omitted for display clarity). Times are displayed in decimal format (e.g., 3.5 is 0330 UTC). The arrow displays direction of propagation. Stations labeled a, b, c, and d are BRIS, OKEM, STUA, and ANTL, respectively. (b) Isochrones of the sharp pressure rise (light gray; 1 h) and temperature drop (dark gray; 1 h) associated with the convective system. The same format as in (a) is used. Stations labeled a, b, and c are CHAN, CALV, and ANTL, respectively.

indicated by the arrow (350°). The times of passage at the stations labeled as a, b, c, and d (BRIS, OKEM, STUA, and ANTL, respectively) were used to calculate an average ground-relative wave speed of 34.1 m s^{-1}. The mean environmental tropospheric wind speed parallel to the direction of wave motion, 1.6 m s^{-1}, was computed using the 0000 UTC sounding from Norman, Oklahoma (KOUN, not shown). Accounting for this tailwind yields an actual wave speed of 32.5 m s^{-1}.

Theoretical gravity wave speed in an atmosphere at rest is given by (Nicholls et al. 1991):

$$c = \left(\frac{NH}{n\pi}\right), \tag{1}$$

where N is the Brunt–Väisälä frequency, H is the vertical depth of the atmosphere, and n is the vertical mode of the temperature perturbation (in this case, a heating perturbation). As suggested in previous studies (Gallus and Johnson 1991; Nicholls et al. 1991), the heating from the convective line has an approximate first internal mode structure ($n = 1$) extending the entire depth of the troposphere. The estimated depth of the troposphere, obtained from visual examination of the 0000 UTC KOUN sounding, is 9.8 km. Using the mean N from the sounding calculated over this depth (0.0129 s^{-1}) yields a wave speed of 40.4 m s^{-1}. This speed is slightly faster than the speed found from surface observations (32.5 m s^{-1}); however, the agreement is reasonable given potential errors in the estimates of N and H. A gravity wave moving at a speed of 32.5 m s^{-1}, at the given N, would require heating over a depth of 7.9 km, which is not an unreasonable estimate of H for this convective system.

b. *Slower-moving surface pressure and temperature disturbance*

Once a bow echo reaches maturity, it is typically associated with both an intense convective line and an extensive stratiform precipitation region. The low-level cooling produced by both features yields a cold pool that spreads outward along the surface, and typically also induces a surface mesohigh (Fujita 1955). The low-level cooling can also generate a slower-moving gravity wave (Nicholls et al. 1991; Fovell 2002). Amplification of the surface mesohigh could occur if the gravity wave is moving at a speed similar to its forcing (the source of the cooling), shown theoretically in the linear analysis of Haertel and Johnson (2000). A strong mesohigh traveling closely with the 13 March 2003 bowing system was evident from 30 min after the formation of the convective line until its dissipation (Figs. 5b–f). However, whether this mesohigh was entirely hydrostatically induced or was partially amplified by a slow-moving gravity wave is uncertain.

The time series from station VANO (Fig. 5) can be examined for evidence of a slow-moving low-level gravity wave or a gravity current. At 0535 UTC, a sharp increase in pressure, a wind shift of almost 180°, and an increase in wind speed all occurred (marked by arrows b and c in Fig. 5), but they were not accompanied by a potential temperature drop. The sharp temperature drop and onset of rain at 0555 UTC (arrows d and e) indicated the arrival of the surface cold pool or gravity current. Both of these features, the sharp pressure increase and sharp potential temperature drop, were noted at almost all stations passed by the bow echo both before and after new bowing developed. Figure 9b shows isochrones of this sharp pressure rise and of the potential temperature drop associated with the arrival of the cold pool. During the initiation phase of the system, the two sets of contours generally appear parallel. However, after new bowing development the pressure rises in some areas occurred well in advance of the potential temperature drop. The dark-gray arrow shows the feature's direction of motion (300°). Times of passage at stations CHAN, CALV, and ANTL (labels a, b, and c, respectively) yield two ground-relative speeds of the leading pressure rise, one prior to most of the new bowing development (from a to b; 10.9 m s^{-1}) and one during bowing (b to c; 21.6 m s^{-1}). The speed of the cold pool was also calculated over the same periods: 11.1 m s^{-1} from stations CHAN to CALV, and 15.8 m s^{-1} from CALV to ANTL. The speeds of the cold pool are very similar to the speeds calculated using the time of first observed precipitation during these same periods: 11.1 and 17.3 m s^{-1}, respectively. Although the division between periods of ''prior to'' and ''during'' bowing is not exact, it is still evident that the pressure rise traveled more quickly than both the cold pool and the leading edge of the precipitation during bowing. This is reflected at the surface by the prebowing mesohigh surge, with the cold pool remaining centered behind the convective line (Fig. 7, stage 2).

These observations could be indicative of a low-level gravity wave moving quickly ahead of the rest of the system, initially generated by an increase in the depth of the low-level cooling within the convective line and stratiform region as the storm develops [see Eq. (1)]. The separation of the sharp pressure rise and wind shift (arrows b and c in Fig. 5) from the potential temperature drop and start of precipitation (arrows d and e) by 20 min also seems to suggest discrete gravity wave and gravity current passages at station VANO. Observations during the 31 May–1 Jun 1969 squall line, analyzed in Charba (1974), exhibited a similar pattern, with the initial sharp pressure rise occurring approximately 10 min prior to the temperature drop at the leading edge of the cold pool. Charba suggested that while it was possible for this surface pressure pattern to be generated by a sufficiently thick layer of cold air aloft moving ahead of the surface cold pool such an occurrence was unlikely because this would result in convectively unstable conditions. Such conditions are unable to persist near ongoing convection for a sustained length of time. Charba theorized that the pressure rise was associated with an elevated gravity wave while the potential temperature drop was a gravity current. However, no observations above 444 m were available in that study. The idealized simulation of a combined gravity current and gravity wave by Haertel et al. (2001) also presented a similar gap between the initial surface pressure rise and potential temperature drop.

Pressure and temperature observations from a gust front on 17 June 1978, analyzed by Wakimoto (1982), also exhibited an approximately 10-min interval between the initial pressure rise and temperature drop. However, it was suggested by Wakimoto that the pressure rise in advance of the cold pool was due to the nonhydrostatic pressure of colliding air masses at the cold-pool interface; Klemp (1994) noted similar behavior in their evaluation of idealized numerical models. Such an effect was not included in the linear simulations of Haertel et al. (2001). If the idea of Wakimoto (1982) and Klemp (1994) is correct, a gravity current alone would be sufficient to produce the pressure and potential temperature time series seen at station VANO. A deepening and/or strengthening cold pool, resulting in a faster-moving gravity current, would be reflected in larger nonhydrostatic pressure perturbations reaching farther from the convective line, much like the observed mesohigh surge. However, whether such pressure rises can reach approximately 50 km ahead of a gravity current is unclear. Moreover, unlike the gravity currents depicted in Wakimoto (1982) and simulated by Haertel et al. (2001), both wind speed and pressure began to decrease just after the time of arrival of the gravity current at VANO.

An additional factor to consider in this case is the increasing stability of the boundary layer in advance of the system as a result of nighttime radiational cooling. Parker (2008) simulated squall-line MCSs encountering a cooled stable boundary layer after reaching maturity. With a conditionally unstable boundary layer, the cold pool spread along the surface as a gravity current. As the stability of the boundary layer increased, the gravity current transitioned to a gravity current disturbance, and then to a gravity wave–like bore. Provided the environment has enough elevated CAPE, the convective system can become entirely elevated, relying on the gravity wave to provide lift. The stable layer beneath the system, if strong enough, can be entirely undisturbed as

the system moves overhead. As the feature evolves into a gravity wave that no longer transports mass, its speed increases. Thus, it also possible that the initial sharp pressure rise observed at VANO is due to a bore or gravity wave propagating along the top of the nighttime stable boundary layer. In this case, cold air was able to descend to the surface through the stable layer as a surface cold pool was observed with a $\Delta\theta$ of 5 K. This surface cooling was not observed in Parker (2008), but Bryan and Weisman (2006) were able to reproduce elevated MCSs with significant surface cold pools provided midlevel low θ_e air was able to descend to the surface.

A recent study by Engerer et al. (2008) used Oklahoma Mesonet data time series to examine characteristics of cold pools associated with squall-line MCSs larger than 200 km. They found that, at the time of squall-line initiation, the mean potential temperature drop as a squall line passed a station was 8.8 K. In this study, the mean potential temperature drop at the time of new bowing development was only 4.3 K, with a standard deviation of 2.2 K. (The temperature drop was calculated using time series data from the station closest to the apex of the bow at the time new bowing development began.) The most likely reason for the smaller temperature drop in this study is the difference in horizontal scale of the systems. Engerer et al. looked specifically at MCSs larger than 200 km, whereas this study only examined systems smaller than 200 km.

It could also be argued that, because 29 of the 39 bowing episodes in this study occurred at night (defined as occurring greater than 30 min after sunset and at least 30 min before sunrise), the increasing stability of a nighttime boundary layer in advance of a bow-echo system would act to decrease the magnitude of the temperature drop. However, in contradiction to this idea, the mean temperature drop of the six daytime bowing episodes (3.4 K) was actually 1.4 K smaller than the mean nighttime episode temperature drop (4.8 K). One possible factor in this result is that new bowing development occurred at different times in the life cycle of the associated convective lines. A temperature drop observed during new bowing development that occurred toward the end of a convective line's life cycle would be expected to be smaller in magnitude than a temperature drop observed at the beginning of its life cycle. The small sample of daytime cases is an additional factor. Thus, conclusions about the importance of a stable boundary layer, in advance of a bow-echo system, to the strength of the surface cold pool cannot be drawn at this time.

It is clear that further research including observations or model simulation of conditions above the surface will be required to examine fully the dynamic processes occurring with the mesohigh surge.

6. Summary and conclusions

This study is directed toward an improved understanding of the behavior of mesoscale surface pressure and temperature anomalies accompanying the initiation, development, and dissipation of bow echoes. Toward this end, Oklahoma Mesonet data have been used to create high-pass, temporally filtered mesoanalyses overlaid on WSI NOWrad composite radar data during 2002–05. This dataset was examined for bow echoes that were both large and long lasting enough to be adequately sampled by the observation network. Surface pressure, temperature, and wind patterns typically associated with bow echoes were identified (see conceptual model in Fig. 7). The following features are noted in each pattern [the phraseology of north (south) is used to refer to the left (right) ends of the line as viewed in the direction of motion]:

1) Stage 1: At some point after convective line formation but prior to bowing development, the mesohigh and cold pool centers are each approximately 50 km behind the line. The cold pool is centered behind the line with the mesohigh slightly farther south. Surface winds in advance of the system are generally southeasterly, providing inflow.
2) Stage 2: The mesohigh surges partially or fully ahead of the convective line, generally south of its center. Bowing of the convective line has typically not yet occurred. The cold pool remains positioned behind the central axis of the convective line. The winds within the pressure gradient on the leading edge of the mesohigh, now ahead of the convective line because of the surge, shift clockwise to become westerly.
3) Stage 3: New bowing develops slightly north of the pressure surge about 0.5 h later. The cold pool remains centered behind the line and expands as the line bows. Winds within the leading mesohigh pressure gradient continue to be westerly, but the convective line begins to eclipse the pressure gradient. Stages 2 and 3 are the pressure surge–new bowing cycle and might repeat multiple times before dissipation.
4) Stage 4: During convective line dissipation, the mesohigh remains slightly south and behind the dissipating bow apex. If the stratiform precipitation region is asymmetric, the mesohigh shifts to the north so that it is more collocated with the most intense portion of the stratiform region. The cold pool in both types stays centered 50–100 km behind the apex. The leading edge of the mesohigh pressure gradient is now typically collocated with the convective line so that winds in advance of the system are entirely southeasterly, providing inflow.

Examination of observed surface time series during the 13 March 2003 bow echo indicated passage of a fast-moving wavelike feature. Hours ahead of the convective line passage, a dip in pressure with little associated change in winds or temperature was noted. This pressure trough, which propagated rapidly away from the initiating convective line at a speed of approximately 34 m s^{-1}, was presumed to be a surface manifestation of a gravity wave generated by deep convective heating in the convective line. This study has provided the first clear observational evidence at the surface of this type of wave.

The same set of time series also exhibited a subsequent wind shift and sharp increase in pressure and wind speed, accompanied by a small temperature drop. After 20 min, precipitation began and the temperature dropped sharply as the surface gravity current arrived. The initial increase in pressure was hypothesized to be due to several possible mechanisms, singly or in combination: 1) nonhydrostatic pressure perturbations due to convergence in advance of the cold pool; 2) a slow-moving gravity wave, presumably generated by low-level cooling within the convective line and stratiform region associated with evaporation of precipitation in the lower troposphere; or 3) an elevated bore propagating along the top of the nighttime stable boundary layer. However, direct observations to substantiate the specific roles of the processes in the pressure surge are currently lacking. Further research is clearly needed to explain these features.

The 2003 BAMEX field campaign provides excellent higher-resolution radar analyses and denser upper-air observations that can be used to better elucidate the bowing mechanisms. A numerical modeling study that explores the relative roles of gravity waves and gravity currents in the mesohigh surge should be a key area of future work. Other remaining questions include the relationship between the mesohigh surge and the development of the stratiform precipitation region, the cause of the bow apex positioning north of the mesohigh surge, and investigation of these gravity wave features in more cases.

It also is difficult at this time to utilize the cycle of pressure surge–new bowing as a forecasting aid for bow-echo development. A surface observation network of sufficient density to resolve the pressure-surge feature would be required. As more mesonetworks are established throughout the country, such a technique would become operationally viable, providing increased lead times for bow-echo and severe convective wind forecasting.

Acknowledgments. This research was supported by National Science Foundation Grant ATM-0500061 and a 1-yr American Meteorological Society graduate fellowship from the ITT Aerospace Communications Division. Oklahoma Mesonet data were provided through the courtesy of the Oklahoma Mesonet, a cooperative venture between Oklahoma State University and the University of Oklahoma and supported by the taxpayers of Oklahoma. The WSI NOWrad data were provided by the Mesoscale and Microscale Meteorology Division of the University Corporation for Atmospheric Research (UCAR) through David Ahijevych. Patrick Haertel assisted with data interpretation. Thanks are also given to Paul Ciesielski, Rick Taft, and Dan Lindsey for assistance in displaying a portion of the data and to Marc Hidalgo for useful discussion. The helpful comments of Matthew Parker and an anonymous reviewer are greatly appreciated.

REFERENCES

Barnes, S. L., 1973: Mesoscale objective analysis using weighted time-series observations. NOAA Tech. Memo. ERL NSSL-62, National Severe Storms Laboratory, Norman, OK, 60 pp. [NTIS COM-73-10781.]

Brock, F. V., K. C. Crawford, R. L. Elliott, G. W. Cuperus, S. J. Stadler, H. L. Johnson, and M. D. Eilts, 1995: The Oklahoma Mesonet: A technical overview. *J. Atmos. Oceanic Technol.,* **12,** 5–19.

Bryan, G. H., and M. L. Weisman, 2006: Mechanisms for the production of severe surface winds in a simulation of an elevated convective system. Preprints, *23rd Conf. on Severe Local Storms,* St. Louis, MO, Amer. Meteor. Soc., 7.5.

——, D. A. Ahijevych, C. Davis, S. B. Trier, and M. Weisman, 2005: Observations of cold pool properties in mesoscale convective systems during BAMEX. Preprints, *11th Conf. on Mesoscale Processes,* Albuquerque, NM, Amer. Meteor. Soc., JP5J.12.

Charba, J., 1974: Application of gravity current model to analysis of squall-line gust front. *Mon. Wea. Rev.,* **102,** 140–156.

Cressman, G. P., 1959: An operational objective analysis system. *Mon. Wea. Rev.,* **87,** 367–374.

Duchon, C. E., 1979: Lanczos filtering in one and two dimensions. *J. Appl. Meteor.,* **18,** 1016–1022.

Engerer, N. A., D. J. Stendsrud, and M. C. Coniglio, 2008: Surface characteristics of observed cold pools. *Mon. Wea. Rev.,* **136,** 4839–4849.

Evans, J. S., and C. A. Doswell, 2001: Examination of derecho environments using proximity soundings. *Wea. Forecasting,* **16,** 329–342.

Fovell, R. G., 2002: Upstream influence of numerically simulated squall-line storms. *Quart. J. Roy. Meteor. Soc.,* **128,** 893–912.

Fujita, T. T., 1955: Results of detailed synoptic studies of squall lines. *Tellus,* **7,** 405–436.

——, 1978: Manual of downburst identification for project NIMROD. SMRP Research Paper 156, University of Chicago, 104 pp. [NTIX PB-28604801.]

Gallus, W. A., Jr., and R. H. Johnson, 1991: Heat and moisture budgets of an intense midlatitude squall line. *J. Atmos. Sci.,* **48,** 122–146.

Glickman, T. S., Ed., 2000: *Glossary of Meteorology*. 2nd ed. Amer. Meteor. Soc., 855 pp.

Haertel, P. T., and R. H. Johnson, 2000: The linear dynamics of squall line mesohighs and wake lows. *J. Atmos. Sci.,* **57,** 93–107.

——, ——, and S. N. Tulich, 2001: Some simple simulations of thunderstorm outflows. *J. Atmos. Sci.,* **58,** 504–516.

Hilgendorf, E., and R. Johnson, 1998: A study of the evolution of mesoscale convective systems using WSR-88D data. *Wea. Forecasting,* **13,** 437–452.

Houze, R. A., M. I. Biggerstaff, S. A. Rutledge, and B. F. Smull, 1989: Interpretation of Doppler weather radar displays of midltatiude mesoscale convective systems. *Bull. Amer. Meteor. Soc.,* **70,** 608–619.

——, B. F. Smull, and P. Dodge, 1990: Mesoscale organization of springtime rainstorms in Oklahoma. *Mon. Wea. Rev.,* **118,** 613–654.

Hoxit, L. R., C. F. Chappel, and J. M. Fritsch, 1976: Formation of mesolows or pressure troughs in advance of cumulonimbus clouds. *Mon. Wea. Rev.,* **104,** 1419–1428.

Jorgensen, D. P., H. V. Murphey, and R. M. Wakimoto, 2004: Rear-inflow evolution in a non-severe bow echo observed by airborne Doppler radar during BAMEX. Preprints, *22nd Conf. on Severe Local Storms,* Hyannis, MA, Amer. Meteor. Soc., 4.6.

Johns, R. H., and W. D. Hirt, 1987: Derechos: Widespread convectively induced windstorms. *Wea. Forecasting,* **2,** 32–49.

Johnson, B. C., 1983: The heat burst of 29 May 1976. *Mon. Wea. Rev.,* **111,** 1776–1792.

Johnson, R. H., and P. J. Hamilton, 1988: The relationship of surface pressure features to the precipitation and air flow structure of an intense midlatitude squall line. *Mon. Wea. Rev.,* **116,** 1444–1472.

Klemp, J. B., 1994: On the dynamics of gravity currents in a channel. *J. Fluid Mech.,* **269,** 169–198.

Klimowski, B. A., 1994: Initiation and development of rear inflow within the June 28–29 North Dakota mesoconvective system. *Mon. Wea. Rev.,* **122,** 765–779.

——, R. Przybylinski, G. Schmocker, and M. R. Hjelmfelt, 2000: Observations of the formation and early evolution of bow echoes. Preprints, *20th Conf. of Severe Local Storms,* Orlando, FL, Amer. Meteor. Soc., 44–47.

——, M. J. Bunkers, M. R. Hjelmfelt, and J. N. Covert, 2003: Severe convective windstorms over the northern high plains of the United States. *Wea. Forecasting,* **18,** 502–519.

Knievel, J. C., and R. H. Johnson, 1998: Pressure transients with MCS mesohighs and wake lows. *Mon. Wea. Rev.,* **126,** 1907–1930.

Lafore, J.-P., and M. W. Moncrieff, 1989: A numerical investigation of the organization and interaction of the convective and stratiform regions of tropical squall lines. *J. Atmos. Sci.,* **46,** 3144–3176.

Loehrer, S. M., and R. H. Johnson, 1995: Surface pressure and precipitation life cycle characteristics of PRE-STORM mesoscale convective systems. *Mon. Wea. Rev.,* **123,** 600–621.

Mapes, B. E., 1993: Gregarious tropical convection. *J. Atmos. Sci.,* **50,** 2026–2037.

Nicholls, M. E., R. A. Pielke, and W. R. Cotton, 1991: Thermally forced gravity waves in an atmosphere at rest. *J. Atmos. Sci.,* **48,** 1869–1884.

Nuss, W. A., and D. W. Titley, 1994: Use of multiquadric interpolation for meteorological objective analysis. *Mon. Wea. Rev.,* **122,** 1611–1631.

Pandya, R. E., and D. R. Durran, 1996: The influence of convectively generated thermal forcing on the mesoscale circulation around squall lines. *J. Atmos. Sci.,* **53,** 2924–2951.

Parker, M. D., 2008: Response of simulated squall lines to low-level cooling. *J. Atmos. Sci.,* **65,** 1323–1341.

——, and R. H. Johnson, 2000: Organizational modes of midlatitude convective systems. *Mon. Wea. Rev.,* **128,** 3413–3436.

——, and J. C. Knievel, 2005: Do meteorologists suppress thunderstorms?: Radar-derived statistics and the behavior of moist convection. *Bull. Amer. Meteor. Soc.,* **86,** 341–358.

Przybylinski, R., 1995: The bow echo: Observations, numerical simulations, and severe weather detection methods. *Wea. Forecasting,* **10,** 203–218.

Rotunno, F., J. B. Klemp, and M. L. Weisman, 1988: A theory for strong, long-lived squall lines. *J. Atmos. Sci.,* **45,** 463–485.

Schmidt, J. M., and W. R. Cotton, 1990: Interactions between upper and lower tropospheric gravity waves on squall line structure and maintenance. *J. Atmos. Sci.,* **47,** 1205–1222.

Skamarock, W., M. Weisman, and J. Klemp, 1994: Three-dimensional evolution of simulated long-lived squall lines. *J. Atmos. Sci.,* **51,** 2563–2584.

Smull, B. F., and R. A. Houze, 1987: Rear inflow in squall lines with trailing stratiform precipitation. *Mon. Wea. Rev.,* **115,** 2869–2889.

Stumpf, G., R. Johnson, and B. Smull, 1991: The wake low in a midlatitude mesoscale convective system having complex organization. *Mon. Wea. Rev.,* **119,** 134–158.

Trapp, R. J., and M. Weisman, 2003: Low-level mesovortices within squall lines and bow echoes. Part II: Their genesis and implications. *Mon. Wea. Rev.,* **131,** 2804–2823.

Wakimoto, R. M., 1982: Life cycle of thunderstorm gust fronts as viewed with Doppler radar and rawinsonde data. *Mon. Wea. Rev.,* **110,** 1060–1082.

——, H. V. Murphey, C. A. Davis, and N. T. Atkins, 2006a: High winds generated by bow echoes. Part I: Overview of the Omaha bow echo 5 July 2003 storm during BAMEX. *Mon. Wea. Rev.,* **134,** 2793–2812.

Wakimoto, R., H. Murphey, C. Davis, and N. Atkins, 2006b: High winds generated by bow echoes. Part II: The relationship between the mesovortices and damaging straight-line winds. *Mon. Wea. Rev.,* **134,** 2813–2829.

Weisman, M., 1992: The role of convectively generated rear-inflow jets in the evolution of long-lived mesoconvective systems. *J. Atmos. Sci.,* **49,** 1826–1847.

——, 1993: The genesis of severe, long-lived bow echoes. *J. Atmos. Sci.,* **50,** 645–670.

——, and R. J. Trapp, 2003: Low-level mesovortices within squall lines and bow echoes. Part I: Overview and dependence on environmental shear. *Mon. Wea. Rev.,* **131,** 2779–2803.